Bay Breeze and Sea Breeze Circulation Impacts on the Planetary Boundary Layer and Air Quality From an Observed and Modeled DISCOVER-AQ Texas Case Study

V. Caicedo[1,2] [ID]**, B. Rappenglueck[1], G. Cuchiara[3,4]** [ID]**, J. Flynn[1], R. Ferrare[5]** [ID]**, A. J. Scarino[5,6]** [ID]**, T. Berkoff[5]** [ID]**, C. Senff[7,8]** [ID]**, A. Langford[7]** [ID]**, and B. Lefer[9]** [ID]

[1]Department of Earth and Atmospheric Science, University of Houston, Houston, TX, USA, [2]Now at Joint Center for Earth Systems Technology, Baltimore, MD, USA, [3]Institute of Arctic and Alpine Research (INSTAAR/CU-Boulder), Boulder, CO, USA, [4]National Center for Atmospheric Research, Boulder, CO, USA, [5]NASA Langley Research Center, Hampton, VA, USA, [6]Science Systems and Applications, Inc., Hampton, VA, USA, [7]National Oceanic and Atmospheric Administration Earth Systems Research Laboratory, Boulder, CO, USA, [8]Cooperative Institute for Research in Environmental Sciences (CIRES), University of Colorado Boulder, Boulder, CO, USA, [9]National Aeronautics and Space Administration Headquarters, Washington, DC, USA

Abstract The role of the sea/bay breeze in the planetary boundary layer evolution and air quality during a high ozone event day in the Deriving Information on Surface Conditions from Column and Vertically Resolved Observations Relevant to Air Quality (DISCOVER-AQ) Texas 2013 campaign was examined. Data from surface air quality monitoring network stations, airborne lidar data, and additional ground-based lidar instrumentation deployed during the campaign allowed for a unique three-dimensional spatial and temporal study of the progression of both meteorological and air quality conditions in the Houston-Galveston regions on 25 September 2013. The Weather Research and Forecasting model coupled with Chemistry model was used to examine the relationship of the land and bay/sea breeze circulations and its influence on air quality during the case study. Comparisons between observations and simulations revealed the largest discrepancies near the Galveston Bay shore areas where the highly localized ozone concentrations were observed and were linked to the strength and timing of the bay/sea breeze progression. Additionally, results indicate vertical downmixing from the remnants of the nighttime residual layer during morning hours into the convective boundary layer and from the lofted offshore return flow into the subjacent bay breeze flow.

1. Introduction

The Houston-Galveston area has been of considerable interest over the past decades as it contains a large and diverse source of emissions from automobiles, power plants, and petrochemical plants combined with complex regional- and local-scale circulations from the nearby Gulf of Mexico and Galveston Bay. These sea breeze and bay breeze circulations play an important role in Houston air quality (Banta et al., 2005; Darby, 2005; Day et al., 2010; Rappenglück et al., 2008, among others). Sea/bay breeze circulations arise from the difference in specific heat of land and water with varying strength depending on body of water size, depth, and geographical environment. After sunrise, due to increased surface heating, air over land will warm faster than air over water. This warm air will eventually rise and allow cooler surface onshore air to move inland, while a warmer offshore return flow can be experienced above. This offshore flow will henceforth be referred to as a lofted return flow (Tijm et al., 1999). After sunset, the air over land cools down more quickly than the air over water. Eventually, a reverse land-to-sea air temperature gradient will create a near-surface return flow. This cool land breeze air will move offshore, replacing the warm air. Both the lofted return flow during the day and the near-surface land breeze at night will have imbedded physical and chemical characteristics, which, once over water, will be exposed to the marine environment. For instance, pollutants will be subject to removal processes, which differ from those over land, as removal from the atmosphere will depend on the water solubility of each individual trace gas. Pollutants with low water solubility such as ozone may not be efficiently removed over water and can be carried back over land with the next day's onset of the sea breeze. In these cases, the land/sea breeze recirculation will not only

alter the planetary boundary layer (PBL) dynamics but can also contribute to increased upwind pollutant concentrations.

Various studies have investigated the meteorological conditions responsible for high ozone events in the Houston-Galveston area, such as those studies performed by Banta et al. (2005) and Darby (2005). Banta et al. (2005) determined that the progression of the sea/bay breeze can simulate a frontal structure along the Galveston Bay/Gulf of Mexico coast and advance inland. The convergence between an offshore synoptic flow and the sea breeze creates a period of stagnation, whose timing and location are determined by the strengths of these counteracting flows, and favors the accumulation of ozone and other pollutants that lead to high ozone concentrations in that area. Similarly, other works such as those of Gangoiti et al. (2002), Darby et al. (2007), Zhang et al. (2007), Wu et al. (2010), Loughner et al. (2014), Stauffer et al. (2013), Martins et al. (2012), and Stauffer and Thompson (2015) have observed links between sea/bay breezes and high ozone in various locations.

Numerical model simulations of these complex land-sea breeze circulations including their strength, and inland propagation has been studied in various locations worldwide. It has been found that they are largely influenced by the prevailing synoptic flow, land/sea surface temperatures, surface winds, and land use and land cover (e.g., Angevine et al., 2006; Bao et al., 2005; Chen et al., 2011; Fast et al., 2006). Studies such as Baker et al. (2013), Loughner et al. (2014), Scarino et al. (2014), and Hegarty et al. (2018) have compared Weather Research and Forecasting model coupled with Chemistry (WRF-Chem) PBL heights with observations relating air quality events to PBL dynamics. Here we use a unique combination of observations and model simulations during complex circulation regimes in order to understand both observed and simulated meteorological circulation impacts on PBL dynamics and chemistry in a coastal region.

In this paper, we will study the effect of the sea/bay breeze on both the PBL evolution and air quality for a high ozone event day (25 September 2013) in the Houston-Galveston area. This day was characterized by a strong sea breeze and bay breeze, similarly to that which occurred during the 30 August 2000 high ozone event day described in Banta et al. (2005). A comprehensive three-dimensional study using both observations and numerical models to investigate the spatiotemporal and vertical evolution of meteorology and air quality has not been performed before in the area. We make use of the extensive data set collected during the DISCOVER-AQ (Deriving Information on Surface conditions from Column and Vertically Resolved Observations Relevant to Air Quality) Campaign. Multiple aerosol backscatter lidars including one airborne lidar were deployed during the campaign allowing for a spatial analysis of the PBL, in addition to an extensive network of air quality monitoring sites already in place in the Houston Galveston area. This study will first analyze the PBL height evolution using ground-based and airborne lidars, trace the concurrent inland progression of the sea/bay breeze as determined by surface wind measurements, and relate these PBL dynamics with air quality conditions in the Houston-Galveston area. We also use the WRF-Chem modeling platform to examine the relationship between the spatiotemporal PBL dynamics, meteorological setup, and the local air quality during sea/bay breeze events.

2. Methods

2.1. Data

The data used in this study were measured within the framework of the NASA DISCOVER-AQ Campaign (data: DISCOVER-AQ Science Team, 2014; https://doi.org/10.5067/Aircraft/DISCOVER-AQ/Aerosol-TraceGas or http://www.air.larc.nasa.gov) in the Houston-Galveston area during the month of September 2013. The overarching goal of this campaign was to improve ground validation of total-column satellite observations related to air quality conditions in the PBL. In this study, we combine Vaisala CL31 aerosol backscatter data measured on the campus of the University of Houston (UH) and on Galveston Island, Micro-Pulse lidar aerosol backscatter data measured at Smith Point, aerosol backscatter and ozone data from the NOAA Tunable Optical Profiler for Aerosol and oZone lidar (TOPAZ) at La Porte, and aerosol backscatter from the NASA High Spectral Resolution Lidar (HSRL-2) aboard the King Air B200 aircraft (Table 1). Surface meteorological and air quality data were provided by the Texas Commission of Environmental Quality Continuous Ambient Monitoring Stations (TCEQ CAMS). Figure 1 shows the locations of ground-based lidars, TCEQ CAMS sites, and the flight tracks of the HSRL. See Supporting Information for a detailed description of the instrumentation.

Table 1
List of Instruments/Platforms and Measured Parameters Used for This Study

Instrument/platform/location	Parameter	Reference
Vaisala CL31 Ceilometer UH campus; Galveston Island	Aerosol backscatter 905 nm	Münkel et al. (2007) and Caicedo et al. (2017)
NOAA Tunable Optical Profiler for Aerosol and oZone (TOPAZ) La Porte	Aerosol backscatter 294 nm and O_3	Alvarez et al. (2011, 2012)
NASA High Spectral Resolution lidar (HSRL) aboard King Air B200	Aerosol backscatter 532 nm	Hair et al. (2008) and Rogers et al. (2009)
Micro Pulse Lidar (MPL) Smith Point	Aerosol backscatter 527 nm	Campbell et al. (2002)
TCEQ CAMS sampling height ~5 m AGL	Ambient temperature, relative humidity, wind speed and direction, O_3, NO, and NO_2	www.tceq.gov/airquality/monops
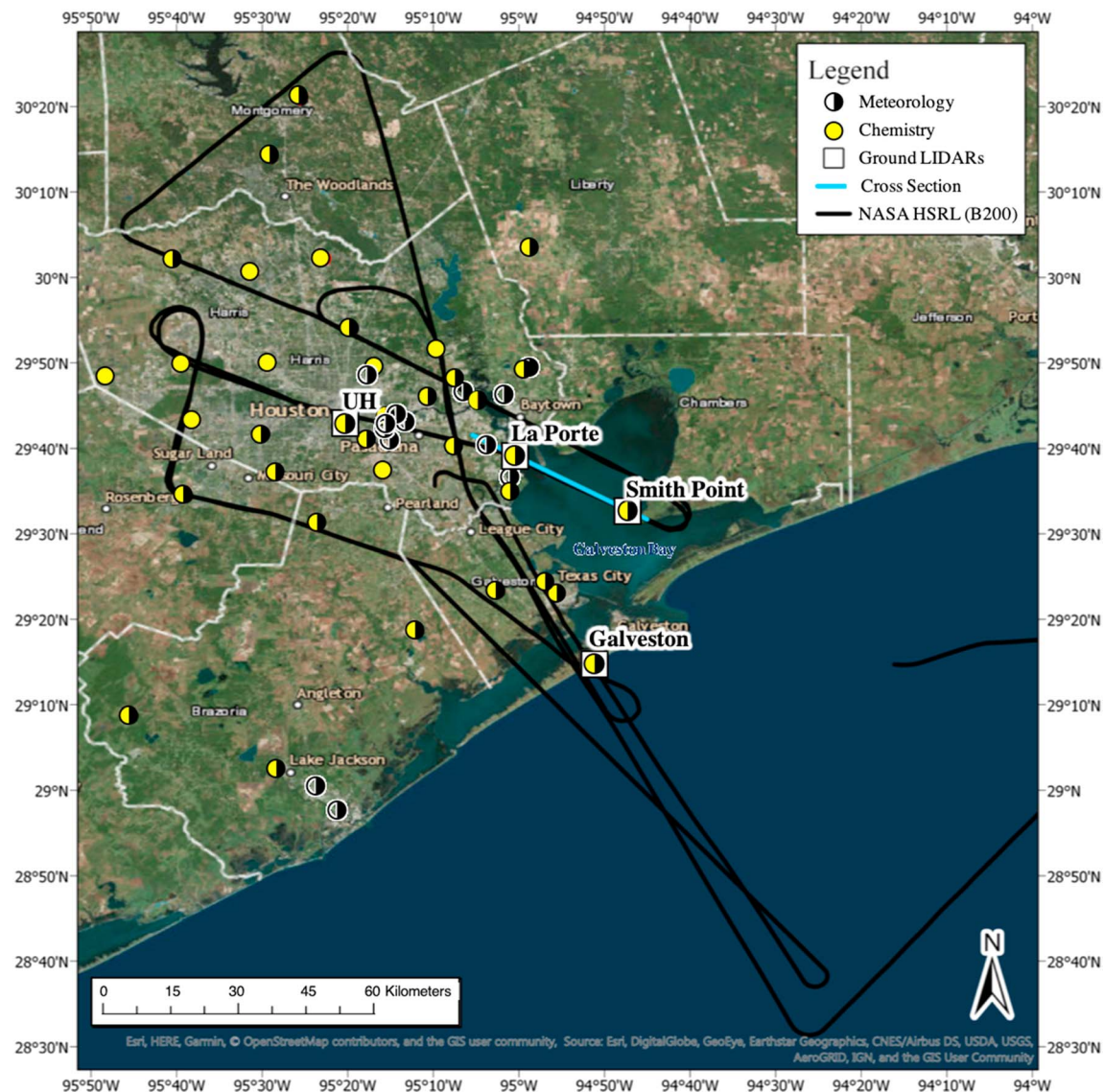
Figure 1. Houston-Galveston area map displaying locations of TCEQ sites with meteorological (half black circles), chemical data (yellow circles), and both meteorological and chemical data (yellow and black circles), ground-based lidar sites (white squares), NASA HSRL-2 aboard B200 aircraft flight tracks on 25 September 2013, in black, and location of cross section discussed in section 4.2 (blue line).

2.2. PBL Height Retrieval Methods

The PBL typically consists of the near-surface nocturnal stable layer (NSL) during nighttime hours and the convective mixed layer (ML) during the daytime. A residual layer (RL) containing remnants of the mixed layer chemical and physical properties is typically found above the NSL. Here we retrieve NSL, RL, and ML heights (collectively referred to as the PBL) from aerosol backscatter lidars (CL31, MPL, TOPAZ, and HSRL-2) using a common Haar wavelet covariance method algorithm described in Caicedo et al. (2017). The common algorithm applies covariance wavelet transforms utilizing the Haar wavelet compound step function (Baars et al., 2008; Brooks, 2003; Caicedo et al., 2017; Cohn & Angevine, 2000; Compton et al., 2013; Davis et al., 2000; Uzan et al., 2016) using several wavelet dilations optimized for each individual lidar in order to identify negative gradients in aerosol backscatter where the local maximum of the gradient is identified as the top of an aerosol layer (Steyn et al., 1999). NSL heights are identified by finding the largest negative gradient closest to the surface, RL heights are identified as the largest gradient above the NSL, and the ML is identified as the overall largest gradient during the daytime. Caicedo et al. (2017) compared PBL height retrievals from over 80 radiosondes and CL31 aerosol backscatter data using three distinct PBL height retrieval methods and found the Haar wavelet method to be the most robust and having the best agreement with radiosonde PBL heights (correlation coefficient of 0.89). Since the late afternoon PBL often becomes stratified with multiple aerosol layers and therefore multiple aerosol gradients, we do not include measurements past 18:00 CST (UTC-6) when the determination of a single mixed layer was not possible. Periods with cloud, rain, and fog signals are not used in the analysis as precipitation signals create large aerosol backscatter gradients that can bias PBL height retrievals. HSRL-2 retrievals use single 532-nm aerosol backscatter profiles in order to reduce spatial averaging when using multiple aerosol backscatter profiles (see Supporting Information). Ground-based lidar retrievals are presented as hourly averages derived from the reported 10-min retrievals for comparison to hourly model outputs.

2.3. Sea/Bay Breeze Identification

The sea and bay breezes are identified using CAMS wind direction, wind speeds, near-surface temperatures, and dew point temperatures. The sea/bay breeze front is identified as a daytime shift into onshore wind direction accompanied by low wind speeds and an increase in dew point temperatures within an hour of the wind shift, while ambient temperatures would remain almost unchanged. For most of the ground sites on the west side of the Bay, the sea breeze will be observed from the SE direction and the bay breeze from the east direction. However, the La Porte site could display both sea breeze and bay breeze from similar directions (see Figure 1 for reference). In this case, we can estimate the time of the sea breeze onset from the inland progression of the sea breeze in nearby CAMS sites (<15 km) that are not influenced by the bay breeze. For this case study, the arrival of the sea breeze front (SE wind direction) was detected at 16:00 CST in the majority of inland TCEQ sites. Therefore, we assume that La Porte did not experience the effect of the sea breeze until 16:00 CST, while the bay breeze was first detected at 11:00 CST. Both times were accompanied by minimal wind speeds, stable near-surface temperatures, and increased dew point temperatures that indicate the arrival of a breeze front.

2.4. WRF-Chem Simulation Characteristics

The WRF-Chem model version 3.7 was used to study the role of the land and bay/sea breeze circulations and its impact on air quality during 25 September 2013. The WRF-Chem grid configuration consists of two model domains using one-way nesting technique with the larger domain centered over the state of Texas (d01 − Δx = 12-km horizontal resolution) and the nested domain (d02 − Δx = 4-km horizontal resolution) centered over the city of Houston (Figure 2). Both domains have 74 vertical levels from the surface to 100 hPa with 12 levels within the PBL (<2 km). WRF-Chem was run for a 72-hr simulation period and initialized on 23 September at 06 UTC, 2013. The first 2 days were considered spin-up; the model results of the last 24-hr simulation period were used for further analysis. The National Centers for Environmental Prediction (NCEP) North American Regional Reanalysis data with 32-km horizontal resolution were used for initial and boundary conditions for the meteorology simulation.

The choice of the PBL scheme for the WRF-Chem simulation was based on previous simulations performed for the Houston-Galveston area such as Czader et al. (2013), Cuchiara et al. (2014), and Wilmot et al. (2014). These studies concluded that the Yonsei University (YSU) scheme is the most suited PBL parameterization
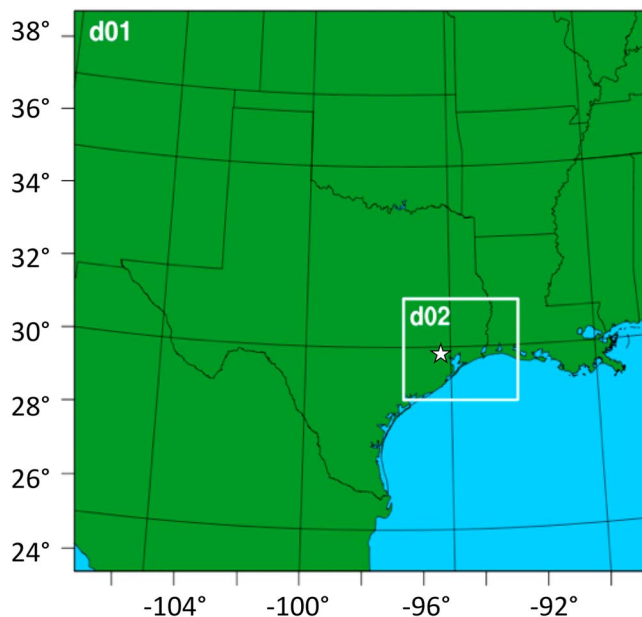
Figure 2. Outer (d01) and nested inner domain (d02) used for the WRF-Chem System.

for the Houston-Galveston area. The YSU is a nonlocal closure model, meaning that it considers fluxes not only of neighboring cells but also other cells in a vertical grid. For this reason, a nonlocal scheme better represents the vertical mixing during convective conditions (Hong et al., 2006). The YSU scheme defines the PBL top as the height where the sensible heat flux reaches a minimum and is identified in the critical bulk Richardson number approaching a zero value (Hong et al., 2006).

The chemistry package of WRF-Chem was turned on for all domains using the Model for Ozone and Related chemical Tracers (MOZART) to represent the gas-phase chemistry and the Global Ozone Chemistry Aerosol Radiation and Transport (GOCART) modal approach for aerosols. The initial chemistry boundary conditions for the chemistry species come from MOZART version 4 global model outputs every 6 hr (Emmons et al., 2010). The Model of Emissions of Gases and Aerosols from Nature (MEGAN) was used to represent the net biogenic emissions, gases, and aerosols in the WRF-Chem model. Anthropogenic emission inventory data were extracted from the U.S. Environmental Protection Agency's National Emission Inventory for the 2011 reporting year. The Fire Inventory from National Center for Atmospheric Research (NCAR) version 1 (FINNv1) was implemented in order to provide daily varying emissions of trace species from biomass burning. Other model configuration details are listed in Table 2.

Statistical analyses were used to evaluate the relationship between hourly air temperatures, winds, sea surface temperature (SST), O_3, NO, and NO_x simulated by WRF-Chem and observed by the CAMS near-surface (sites <15-m above ground level [AGL]) and airborne measurements on 25 September 2013. The statistical parameters included the correlation coefficient (r^2) to determine the strength of linear association between simulation and observations, the root-mean-square error (RMSE), mean absolute error (MAE), mean observed (MO), mean model (MM), and mean bias (BIAS) calculated as the difference between simulation and observations to describe the magnitude of the difference between predicted and observed results.

3. Case Study

Here we present the case study of 25 September 2013 when a strong sea breeze from the Gulf of Mexico in combination with a Galveston Bay bay breeze made their way across the Houston-Galveston area. The effect

Table 2
WRF-Chem Configuration Characteristics

| Domain	d01	d02
WRF-Chem version	3.7 (released April 2016)	
Simulation period	From 23 September at 06 UTC to 26 September at 06 UTC	
Initial condition meteorology horizontal resolution	12 km	4 km
Grid points (x, y)	161 × 145	97 × 79
Microphysics	Lin scheme	
Shortwave/longwave radiation	Rapid Radiative Transfer Model (RRTM)	
Surface layer	Monin-Obukhov with Carlson-Boland viscous sublayer	
Land surface option	Unified Noah Land Surface Model	
Boundary layer	YSU	
Cumulus cloud	Kain-Fritsch	
Initial condition chemistry	MOZART-4	
Chemistry mechanism	MOZART	
Biogenic emissions	MEGAN	
Anthropogenic emissions	NEI2011	
Wildfire emission	FINNv1	
Aerosols option	GOCART	
Land Mask/Geo. classification	24 categories	
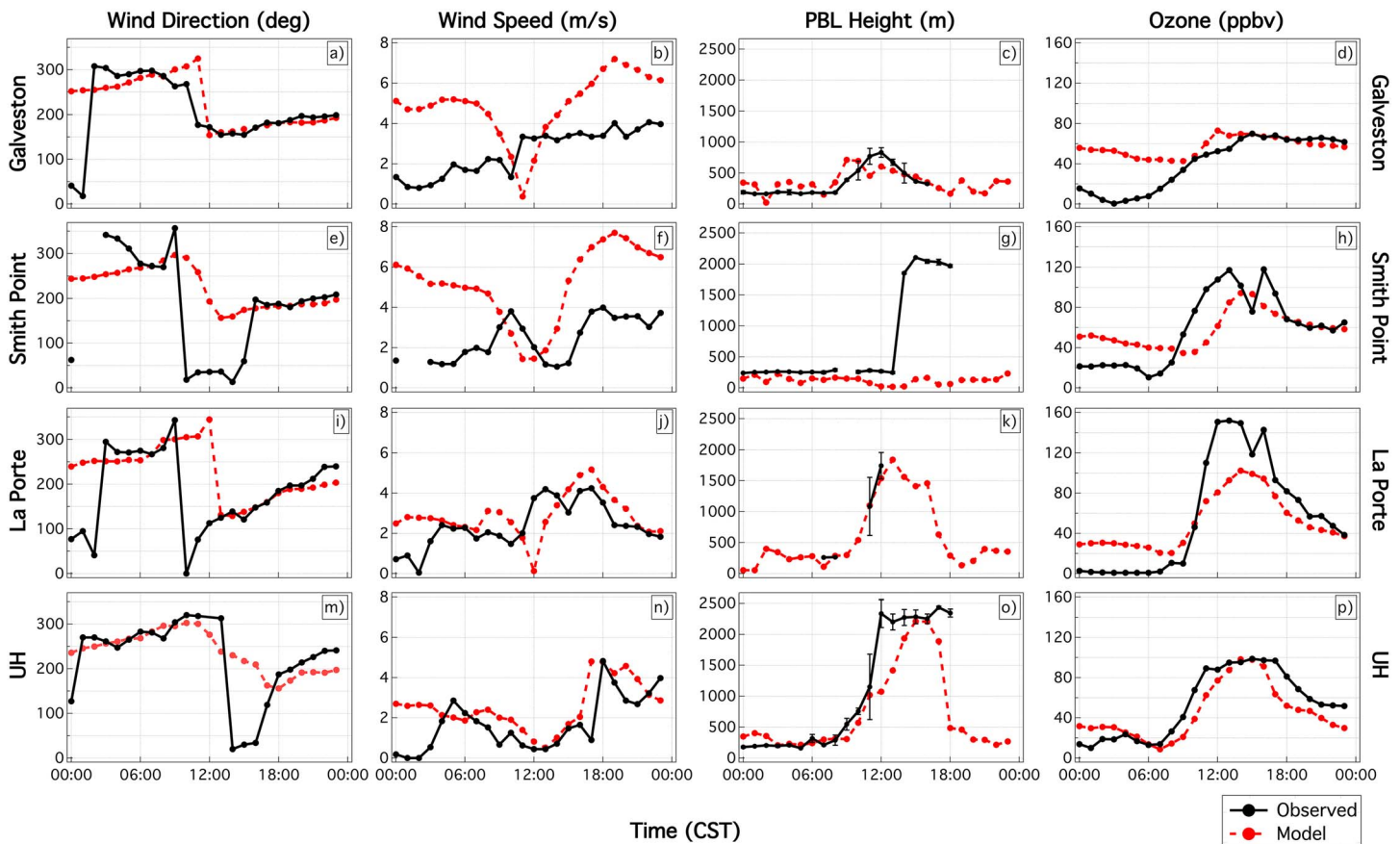
Figure 3. Hourly modeled and observed wind direction, wind speed, PBL heights, and ozone mixing ratios at Galveston (first row; a, b, c, and d), Smith Point (second row; e, f, g, and h), La Porte (third row; i, j, k, and l), and UH campus (lowest row; m, n, o, and p) respectively.

of these flow systems on the spatial and temporal evolution of the PBL and on the air quality in this area is studied. TCEQ CAMS sites are used to detect the progression of the sea/bay breeze with a focus on the lidar ground sites in order to interpret the interactions between the sea/bay breezes and the lidar-retrieved PBL heights. The airborne lidar aids in the connection of spatial PBL dynamics between lidar sites. TCEQ CAMS sites are also used to study the air quality in the area during the high ozone event of 25 September 2013. The case study is analyzed in the following sequence: (1) discussion of meteorological observations, (2) analysis of air quality data, and (3) application of the WRF-Chem model to improve the understanding of the spatiotemporal PBL variability in a complex coastal area and its implication for urban air quality.

3.1. Ground-Based and Airborne Observations

The CAMS surface (~5 m AGL) and profiler upper air wind measurements from 25 September 2013 show similar synoptic winds from the north and west directions with typical speeds below 2 m/s (1.3 m/s on average) during the nighttime and morning hours before the onset of the sea/bay breeze (Figures 3 and 6); note that simulation results are discussed in section 3.2. Low wind speeds observed throughout the nighttime and morning were generally from the W/NW direction, indicating a nighttime land breeze (Figures 3a, 3b, 3e, 3f, 3i, 3j, 3m, and 3n). Banta et al. (2005) noted that similar offshore flows may carry chemically aged air masses over water, which could then be brought back over land with the onset of the daytime sea breeze. NSL heights obtained at Galveston and UH show averaged heights of 180 ± 11.7 and 209 ± 47 m AGL, respectively. NSL heights at Smith Point (Figure 3g) must be carefully used due to limitations from low-resolution and/or unreliable near-ground measurements (<90 m) of the MPL instrument [see Supporting Information]. Therefore, the NSL heights measured by the MPL could be overestimated similar to findings in Hegarty et al. (2018). There were no nighttime TOPAZ measurements at La Porte on 25 September (Figure 3k).
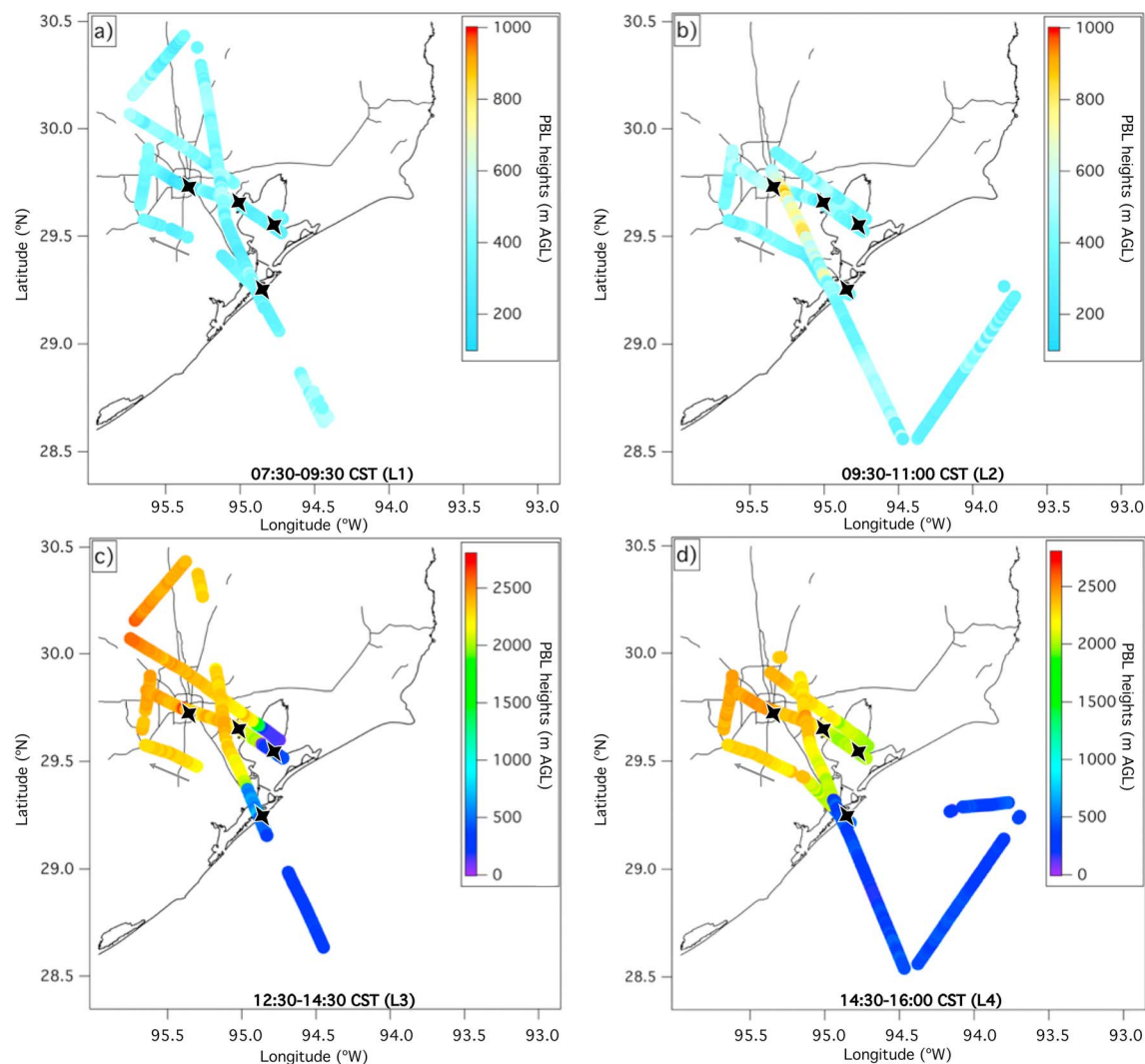
Figure 4. PBL heights derived from the HSRL-2 on 25 September 2013 divided into individual Houston-Galveston area loops L1-L4 at (a) 07:30–09:30 CST (L1), (b) 09:30–11:00 CST (L2), (c) 12:30–14:30 CST (L3), and (d) 14:30–16:00 CST (L4) on 25 September 2013. Grey arrows indicate flight direction. The black markers show (from top to bottom) the locations of the lidars at UH, La Porte, Smith Point, and Galveston.

The initial growth of the convective mixing layer was detected at about 08:00 CST by both UH and Galveston CL31 ceilometers. Fog near the Galveston Bay initially limited the MPL and TOPAZ measurements in the morning from about 9:00–10:00 CST (Figures 3g and 3k). After the fog cleared, the MPL at Smith Point displayed stable PBL heights similar to those observed at the Galveston site, which are attributed to the proximity to water. These sites are closely surrounded by the Galveston Bay and Gulf of Mexico and could mimic marine PBL heights accounting for the stable morning time measurements observed in Figures 3c and 3g.

Airborne HSRL-2 measurements closely follow results found by the ground-based lidars. We divide the HSRL-2 measurements into four flight loops around the Houston-Galveston area (L1–L4). The earliest HSRL-2 loop (L1) was performed from ~7:30 to 09:30 CST (Figure 4a) and shows average PBL heights of 470 ± 64 m AGL over the Gulf of Mexico, 460 ± 28 m AGL over the Galveston Bay, and 358 ± 58 m AGL over land. The second HSRL-2 loop (L2) starts at approximately 9:30 CST and finishes its trajectory at 11:00 CST (Figure 4b). Here, HSRL-2-measured PBL heights over the Gulf of Mexico and Galveston Bay were relatively constant at an average of 430 ± 53 and 388 ± 52 m AGL. PBL heights over land in L2 are higher (564 ± 155 m AGL) and slightly more variable than that of L1, likely due to stratification of aerosol during the time the ML is developing and not yet well mixed creating multiple layers (Figure 4b). The last section of the HSRL-2 trajectory from the Houston downtown area to the Gulf of Mexico in L2 shows PBL heights that

are significantly higher than those measured during L1 (up to ~700 m AGL) and decrease with closer proximity to the Gulf of Mexico. There are no HSRL-2 measurements until about 12:30 CST, and by this time most of the ground-based lidars (Figures 3g, 3k, and 3o) display a sharp increase in PBL heights.

As the bay breeze and sea breeze begin, lidar retrievals display a close relationship between MLH growth and these breezes. Beginning with the Galveston site (first row in Figure 3), the initial onset of the sea breeze (SE winds) occurs ~11:00 CST (Figure 3a). This coincides with the daytime maximum hourly average MLH of 834 $\pm$ 78 m AGL at 12:00 CST (Figure 3c), along with a decrease in MLHs after 12:00 CST. This is likely due to the strengthening of the sea breeze, which essentially pushes air masses inland and replaces them with cooler marine air (Strawbridge & Snyder, 2004). This is also indicated by near-surface temperatures remaining relatively constant (~31 °C), while dew point temperatures increase during and after the sea breeze onset at that site. For the same reason, the sea breeze could inhibit the full PBL growth and eventually lead to decreasing PBL heights at this site (13:00 CST). Farther inland, the Smith Point MPL shows relatively constant heights through 13:00 CST that are attributed to the stabilizing influence of the nearby Galveston Bay.

On the opposite side of the bay, the La Porte site displays the onset of the bay breeze (east direction) at about 11:00 CST. Afterward, winds gradually shift farther to SE as the Gulf sea breeze arrives at La Porte (Figure 3i) by 16:00–17:00 CST. The limited data set from TOPAZ reveals a growth in MLHs with increasing winds following the arrival of the bay breeze. The UH CL31 being the most inland ground-based lidar, shows N/NW winds until about 17:00 CST. At that time winds start shifting to S/SE directions and wind speeds slightly increase to about 3–4 m/s (Figures 3m and 3n) indicating that the sea breeze did not reach this most northern ground-based lidar site until about 17:00 CST. As noted above, CL31 retrievals at the UH site show the initial growth of the ML at about 8:00 CST reaching a maximum MLH of 2,436 $\pm$ 21 m AGL around 12:00 CST.

The two lidar sites near the Galveston Bay shoreline (Smith Point and La Porte) show a sudden and sharp increase in ML heights (Figures 3g and 3k) that also coincides with a significant increase in ML heights over the entire bay as measured by the HSRL-2 (Figures 4c and 4d). A closer look into the aerosol backscatter over that area reveals a significant aerosol loading between 1,300 and 2,000 m AGL and extending from the inland area over the La Porte site outward toward Smith Point (Figure 5a). This layer of aerosols is not directly above the Smith Point site where the ML heights are detected at the lowest gradient (248 $\pm$ 17 m AGL by the MPL and ~360 m AGL by the HSRL). The next HSRL-2 transect (L4) over the same area an hour later at 15:00 CST (Figure 5b) shows relatively uniform aerosol loading from about 400 to 2,000 m above the surface. This causes the PBL algorithms to retrieve the PBL at the large negative gradient near the top of this aerosol layer at 2,055 m AGL by the HSRL-2 and 2,100 m AGL by the MPL (Figure 3g). Although the La Porte site is surrounded by a significant concentration of emission sources (i.e., petrochemical plants), near-surface horizontal transport over the Galveston Bay toward Smith Point is unlikely as the prevalent bay breeze flow is in the opposite direction, that is, from SE (Figures 3i and 6). Additionally, convective mixing over a body of water could not account for the increase in depth of aerosols in Figure 5a compared to that of Figure 5b, as the more stable marine PBL should keep aerosols at lower altitudes. For these reasons, both horizontal (toward the SE/E direction) and turbulent vertical transports over the Galveston Bay are suspected at this site.

Wind profiler measurements from the nearby La Porte site further support this conclusion by revealing a shift to W/NW winds beginning around 11:00 CST at altitudes above ~500 m that indicate a return flow above the bay breeze (Figure 6a). As the HSRL-2 travels from the La Porte toward the Smith Point site (Figures 5a and 5b), we can make a connection between these two sites and conclude that the higher aerosol backscatter over Smith Point can be attributed to a lofted return flow from land above the bay breeze flow.

Figure 5b (~15:00 CST) also reveals the marine ML as a near-surface area of lower aerosol backscatter, below the intruding aerosol backscatter over Galveston Bay between the La Porte and Smith Point sites. The offshore transport occurs above the clean marine boundary layer across the bay and does not entirely replace the marine BL but is instead advected above the marine BL. This implies that the aerosol mixing does not reach the lowest altitudes over the Galveston Bay and does not replace/intrude on the marine ML at this time. As we define the aerosol backscatter PBL height as a strong negative gradient in aerosol backscatter,
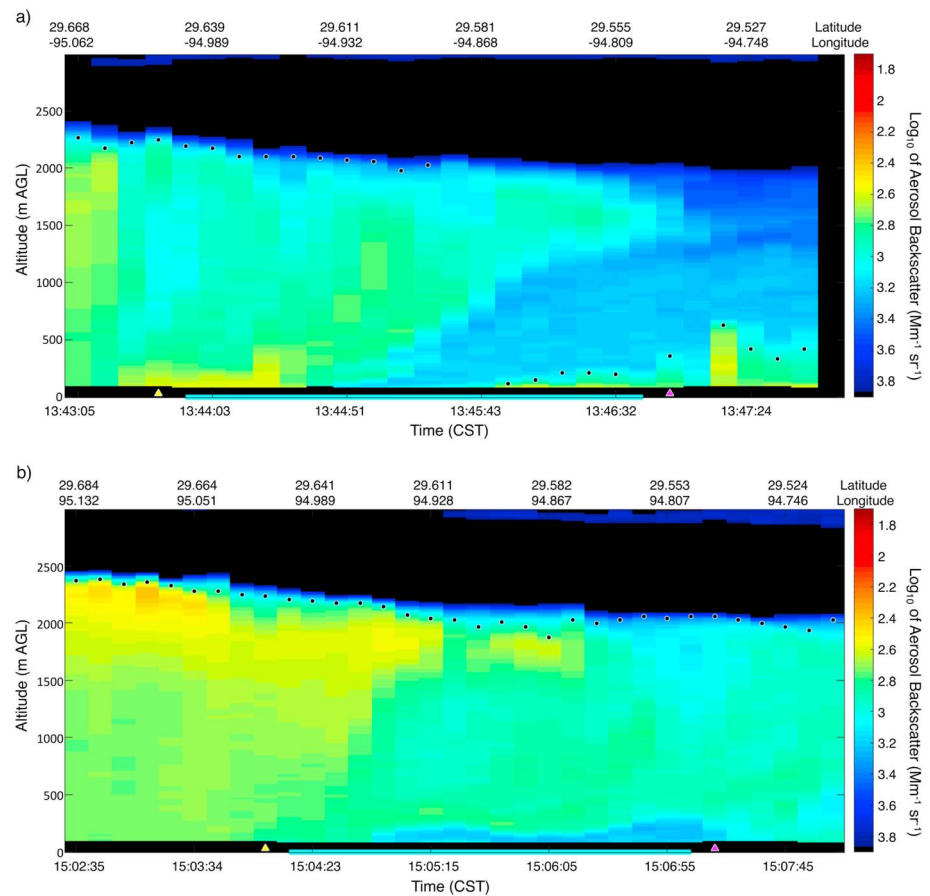
Figure 5. HSRL-2 aerosol backscatter from La Porte to Smith Point: (a) measurements taken at about 13:45 CST and (b) measurements taken at about 15:05 CST on 25 September 2013. PBL heights are displayed as black circles. Yellow and magenta triangles indicate La Porte and Smith Point sites, respectively. The cyan line at 0-m altitude indicates measurements over Galveston Bay.
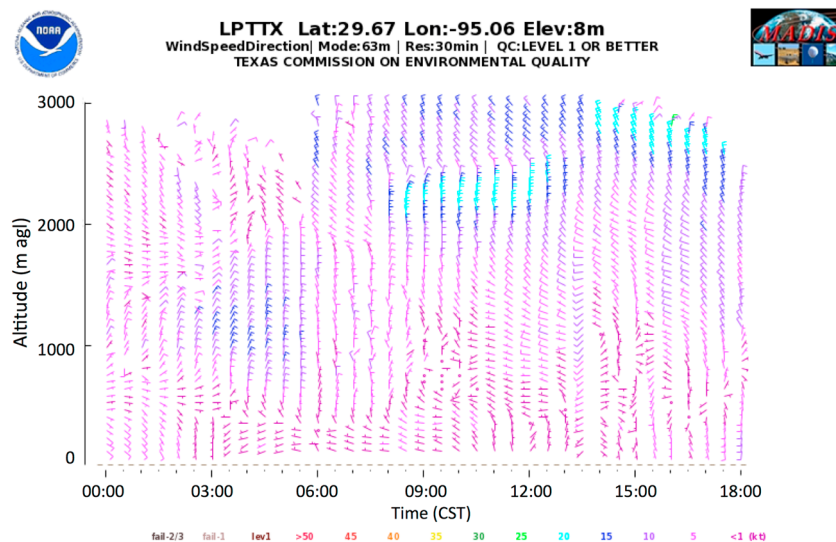
Figure 6. Wind profiler plot for 25 September 2013 measured at La Porte, TX.

the clean (i.e., having lower aerosol backscatter) shallow layer is not identified as a PBL candidate; hence, all lidar retrievals identify the top of the aerosol layer as the MLH (~2,300 m).

After the last HSRL-2 measurement (L4 concluded at ~16:00 CST), we turn to Smith Point MPL ground-based measurements where the area of lower aerosol backscatter (marine BL) is no longer detected. Instead, aerosol backscatter is well mixed up to ~2,300 m. This is key as it points to a succession of vertical distributions between flows. Figure 5a displays the beginning of a relatively high aerosol content offshore flow lofted above the bay breeze flow extending inland and over the Galveston Bay. Approximately an hour afterward, Figure 5b shows significant aerosol loading reaching lower altitudes than those of Figure 5a, yet not fully reaching the Galveston Bay surface. MPL measurements after 16:00 CST show no vertical aerosol layering (i.e., no low aerosol content near the surface) pointing toward the increased vertical transport of the offshore return flow over the Galveston Bay. In these cases, surface measurements taken at coastal sites such as Smith Point must be carefully analyzed as the measurements taken at any time could be indicative of a marine boundary layer or of offshore polluted transport. Furthermore, numerical model simulations must have the ability to differentiate the spatial and vertical distribution of breeze and offshore return flows. In these cases, continuous monitoring of the boundary layer with profiling instrumentation such as remote sensing lidars or ceilometers is crucial.

Previous high ozone event studies in the Houston area (Banta et al., 2005; Darby, 2005) determined that the late onset and inland progression of the sea breeze plays a key role in high ozone events. The location of the convergence between an offshore synoptic flow and the sea breeze causing stagnation needs to be (1) located near pollution sources to allow for the accumulation of emissions and (2) occur during photochemically favorable times (i.e., daytime high solar radiation and temperatures). Additionally, Banta et al. (2005) pointed to the sea breeze-driven return of pollutants previously transported offshore during the nighttime and morning land breeze. This recirculation can contribute to additional pollutant concentrations during the day and enhance the formation of secondary pollutants such as ozone. The measured nighttime and early morning O_3 mixing ratios for this case study remained <10 ppbv over the entire region as displayed in Figure 7 by the circular markers (simulation results will be discussed in section 3.2).

Ozone concentrations began to rise in the Houston-Galveston area around 10:00 CST with a clear localized increase along the western shore of the Galveston Bay as detected by the TCEQ CAMS measurements (Figures 7e to 7i). Ozone concentrations at La Porte increased from 46 to 110 ppbv between 10:00 and 11:00 CST with the onset of the bay breeze (wind shift from north at ~2 m/s to east winds at ~2 m/s), pointing toward a rapid accumulation of emissions in a larger area surrounding the La Porte site after the convergence of opposing flows leading to calm winds. While the La Porte site is located in a residential area, it is about 2 km from the Barbours Cut Terminal, one of the busiest ports worldwide, about 8 km away from Baytown industrial facilities, and it is the closest air quality monitoring site to the Houston Ship Channel entryway. The highest hourly ozone of 151 ppbv at 13:00 CST was found at La Porte (Figure 7g), where multiple petrochemical plants are located. This is also reflected by the vertical enhancement of aerosols measured by both ground-based and airborne lidars. Additionally, the highest ozone (13:00 CST) was measured after the onset of the bay breeze (11:00 CST) and before the arrival of the sea breeze (16:00 CST). In contrast, Banta et al. (2005) observed both bay breeze and sea breeze later in the day at about 15:00 and 18:00 CST, respectively. In this case study, we can conclude that an earlier onset of breeze circulations can also lead to high ozone events and that the nighttime land breeze and daytime bay breeze circulations may facilitate localized high ozone events in the western Galveston Bay.

3.2. WRF-Chem Simulation

The use of the numerical model simulation is twofold: (1) to explain the airborne observations involving the vertical distribution between a return flow and bay breeze (Figures 4 and 5) and (2) subsequently analyze WRF-Chem poor air quality condition events under the impact of complex local circulations.

The simulations overestimate the nighttime winds (Figures 3b, 3f, 3j, and 3n) but present similar wind biases for coastal regions including the Houston area as was found in previous studies such as those by Misenis et al. (2006), Cheng and Steenburgh (2005), Roux et al. (June 2009), Yerramilli et al. (2010), Ngan et al. (2012), and Cuchiara et al. (2014). In the model, the arrival times of the sea and bay breezes are about 2 hr later when compared with the observations (Figure 3). Note that during the onset/arrival
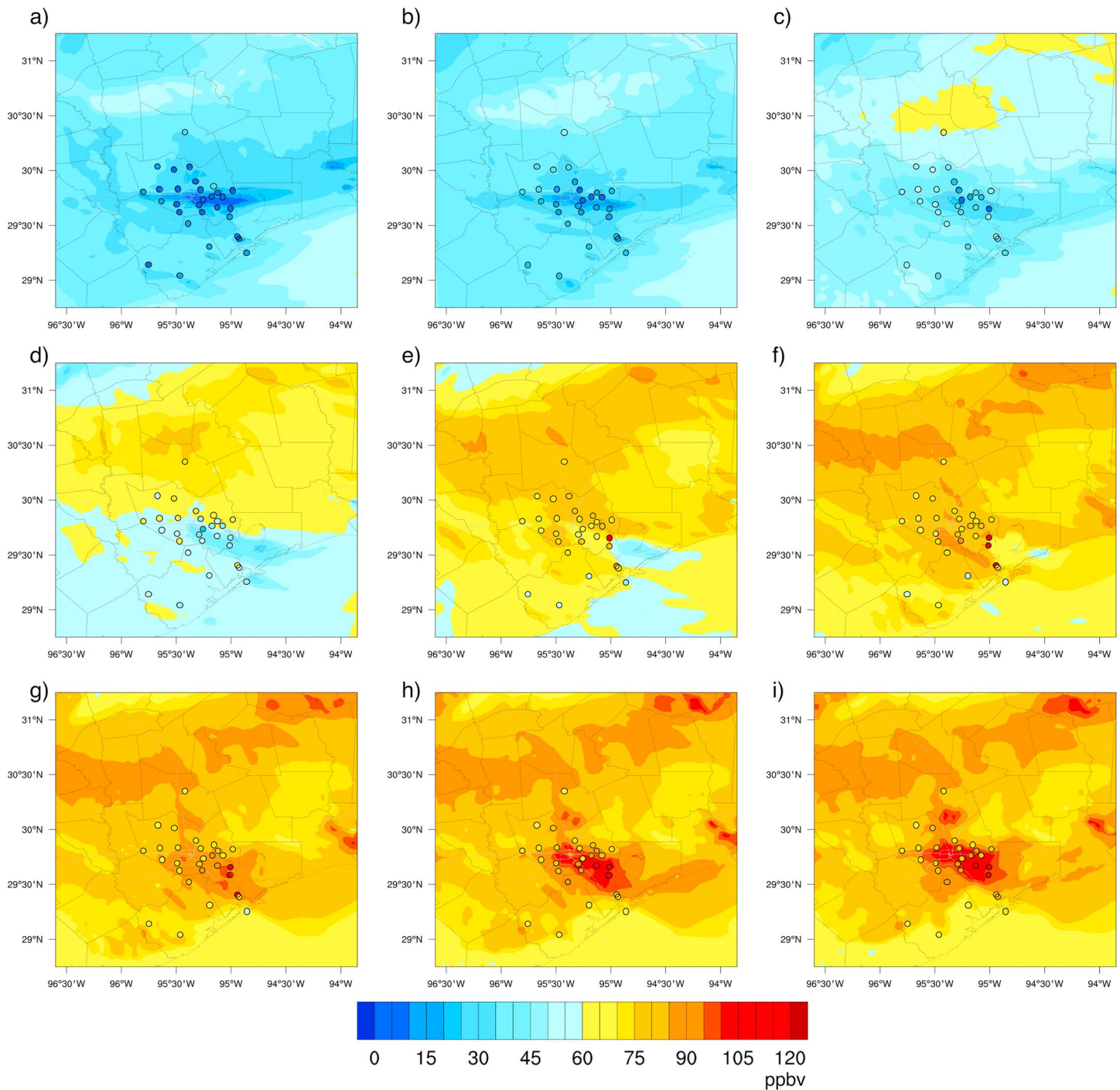
Figure 7. CAMS-measured O$_3$ mixing ratios in ppbv and WRF-Chem results for 07:00 (a), 08:00 (b), 09:00 (c), 10:00 (d), 11:00 (e), 12:00 (f), 13:00 (g), 14:00 (h), and 15:00 CST (i) on 25 September 2013.

of the sea breeze, hourly model output wind speeds decrease to nearly 0 m/s at the sites closer to water. However, near-surface wind measurements do not show such a low hourly averaged wind speed during the onset of the sea breeze.

The sea breeze development occurs as a result of differential heating of air over land and water surfaces. As the air over land quickly heats up and consequently rises, the cool marine air is pulled inland to replace those rising air masses. We use the model 2-m near-surface temperatures and model SST as an indication of the

temperature gradients used to determine the sea breeze strength and inland propagation (Chen et al., 2011; Pendergrass et al., 2010; Steele et al., 2013). Buoy SST data from the U.S. National Data Buoy Center (http://seaboard. ndbc.noaa.gov) and near-surface temperatures close to the Gulf coast are used for model comparison. Observed SST within the simulation domain (one buoy available) was averaged to a daily value to compare with model SST. Although one buoy is used, comparison to model SST can give us an indication of large differences. In addition, the default treatment of SST in WRF-Chem involves assigning the input SST field (from North American Regional Reanalysis 32-km input data) to corresponding water grid cell points in the model domain; therefore, SST at each grid cell does not vary with time over the entire model run. Here we use the closest grid cell to the buoy location. Model SST was slightly higher (29.1 °C) than the daily averaged observed SST of 28.3 °C, while near-surface temperatures displayed good agreement with observed land near-surface temperatures (bias of 0.08 °C). However, hourly correlations point to disparities between model and observations in the early morning hours (Table 5 and S2). This is critical timing for the initiation of surface heating and could therefore explain the difference in timing between observations and model as incorrectly simulated temperature gradients can lead to incorrect timing and inland progression of sea/bay breezes.

Simulated PBL heights were determined as described in section 2.4. Here, we use modeled 2-m air temperatures as a proxy for the land surface sensible heat fluxes as an input for simulating the PBL heights and compare them to observed TCEQ CAMS 10-m temperatures. We expect that higher near-surface temperatures will lead to greater simulated surface fluxes and therefore higher modeled convective PBLs although other influencing factors such as wind speeds and surface roughness cannot be ruled out (Hu et al., 2010; Steele et al., 2013).

Time series of simulated PBL heights and ground-based lidar measurements (Figures 3c, 3k, and 3o) show reasonably good agreement between observations and simulated PBL heights with slight differences in timing. The Smith Point site shows the largest disparity between measurements and model (Figure 3g). This is consistent with its location on a peninsula, which likely leads to lower and more stable PBLs compared to inland areas. However, the MPL at Smith Point measured a sharp increase in the PBL when a strong return flow moved air masses with higher PBL heights and higher aerosol backscatter over the site. This return flow is, in fact, simulated by the model (discussed later in this section), yet the model PBL height remains at low altitudes (Figure 3g). This is a result of the different methods for determining PBL heights used in the observations and the PBL schemes (McElroy & Smith, 1991; Seibert et al., 2000). In this case, the observed PBL heights are calculated at the top of the lofted return flow (largest aerosol gradient), while the model identifies the PBL as the level of lowest surface heat fluxes. Nevertheless, both heights are crucial as observations in this study show that the boundary between these two flows becomes progressively lower in altitude and can therefore have varying effects on pollutant mixing ratios and potential vertical downmixing of pollutants to the surface.

Figure 8 represents simulated PBL heights and overlaid observations from the HSRL-2 measured in the hour of the model output (i.e., a 07:00 CST figure displays HSRL-2 data measured from 07:00 to 07:59 CST). Table 3 gives a statistical analysis of a model-observation comparison. HSRL-2 ML heights are used for ML comparisons and 36 TCEQ ground sites are used for near-surface temperature comparisons. Airborne HSRL-2 PBL heights were compared to the corresponding simulated PBL at the location of each HSRL-2 measurement (note that multiple HSRL-2 measurements can fall into the same grid cell). The simulated boundary layer height at each observation location was chosen at the hour of the measurements (i.e., a 14:40 CST measurement from the HSRL-2 was compared to a 14:00 CST simulated PBL at the same location as the HSRL-2 measurement). No averaging is applied to aircraft PBL observations as this would also create a spatial averaging of the PBL. Temperature observations are hourly averaged and then compared to the model results.

Overall, model near-surface temperatures and PBL heights correlate well with observations with correlations coefficients r^2 of 0.82 and 0.73, respectively, yet near-surface temperatures showed a slight overprediction of 0.08 °C and model ML heights were lower than those measured by the HSRL-2 with a bias of −312.36 m. As the HSRL-2 measures over both water and land from 07:30 to 16:00 CST, we further divide this analysis by land cover (Table 4) and hourly analysis (Table 5). A more detailed analysis is presented in the Supporting Information. As the diurnal evolution of both near-surface temperatures and PBL heights can
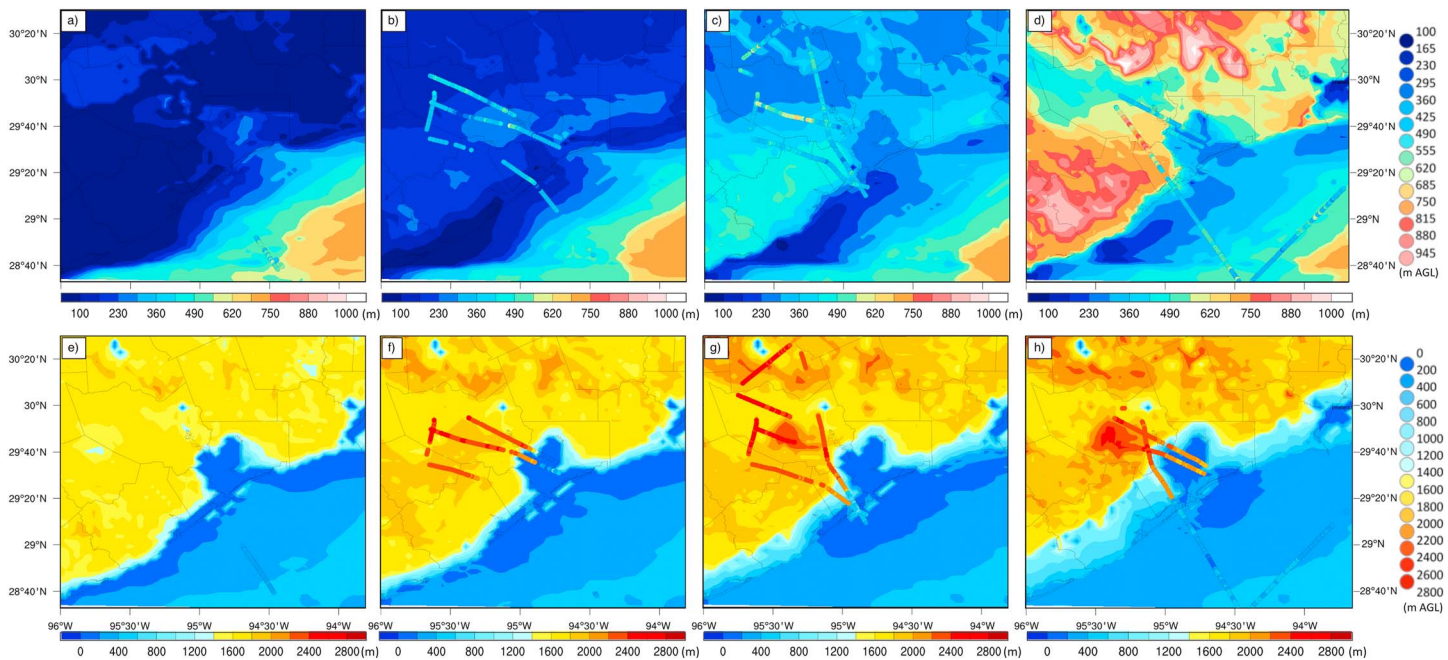
Figure 8. Model PBL heights and corresponding HSRL-2 PBL heights (m AGL) measured at (a) 07:00, (b) 08:00, (c) 09:00, (d) 10:00, (e) 12:00, (f) 13:00, (g) 14:00, and (h) 15:00 CST, on 25 September 2013.

improve correlations between model and observations, the mean bias gives more relevant information regarding the performance of the simulation. Results show that the modeled YSU PBL heights over land were lower than observed (Table 4) and typically accompanied by an underprediction of near-surface temperature during daytime hours (Table 5 and Table S21). This suggests that the low PBL heights may be caused by underestimation of the surface heat fluxes. Results also point to a clear difference in daytime simulated PBL heights over land and water surfaces, with overestimation and, at times, no correlations of simulated PBL heights over the Gulf of Mexico (mean bias of −1.7 m and a correlation coefficient of 0.09), compared to the higher correlation and higher mean bias seen in the measurements over land (correlation coefficient of 0.82 and mean bias of −384.7 m). The slight overestimation and low correlations of simulated PBL heights over the Gulf of Mexico are in line with the model overprediction of SSTs compared to the buoy data. Low PBL correlations between the model and observations over water are also expected due to small variations in the spatial and temporal evolution of the marine boundary layer. Another significant underestimation (bias of −707.6 m and r^2 of 0.03) of the PBL is over the Galveston Bay, Table 4. This is due to the observed return flow over this area that is identified as the PBL (see sections 1.2 and 1.3).

Hourly averages show that the simulated near-surface temperatures were slightly overpredicted during nighttime hours (0:00–6:00 CST) with a bias of 1.06 to 0.17 °C (Appendix B). After sunrise (~7:00 CST), the model underpredicts near-surface temperatures, with the highest underpredictions from ~08:00 to 09:00 CST (bias −1.2 to −1.5 °C). The hourly bias between observed and model PBL heights (Table 5) shows seemingly uncorrelated PBL height and near-surface temperature biases. However, it is important to note that HSRL-2 measurements cover both land and water surfaces, while near-surface temperatures are

Table 3
Statistical Analysis of Simulated and Observed Near-Surface Temperatures, PBL Heights, and Ozone Mixing Ratios

Parameter	r^2	Mean bias	Mean observed	Mean model
Near-surface air temperatures	0.82	0.08 (°C)	27.6 (°C)	27.7 (°C)
PBL heights	0.73	−312.36 (m AGL)	1,031.4 (m AGL)	719.0 (m AGL)
O_3	0.70	10.86 (ppbv)	40.9 (ppbv)	51.5 (ppbv)

Note. Correlation coefficient (r^2), mean bias, and observed and modeled mean values.

Table 4
Correlations Between HSRL-2 and Model-Simulated ML Heights Separated Over Land, Gulf of Mexico, and Galveston Bay Regions

Location	r^2	RMSE (m AGL)	MAE (m AGL)	Mean bias (m AGL)	MO (m AGL)	MM (m AGL)
Gulf of Mexico	0.09	119.2	98.3	1.7	376.8	371.8
Galveston Bay	0.03	1,104.7	747.3	−707.6	1,022.2	337.8
Land	0.82	571.2	408.6	−384.7	1,343.7	917.0

exclusively over land surfaces. Measurements at 7:00, 10:00, and 12:00 CST are taken mostly if not entirely over water and display the largest overpredictions in PBL heights, while the remaining hourly measurements are largely land measurements and display underpredictions of PBL heights.

The largest underpredictions of near-surface temperatures occur in the morning hours from 08:00 to 09:00 CST (Table 5), a time period that is closely associated with the beginning of the PBL growth (cf. Figure 3). These times are vital to the development of the PBL as an underprediction of surface heat fluxes during the morning will limit the vertical mixing of the convective ML and hence the subsequent daytime PBL heights (Strawbridge & Snyder, 2004). Correlations between measured and simulated PBL heights over land show consistently higher values later in the day (maximum r^2 of 0.70 at 13:00 CST, then slightly decreasing to 0.38 at 15:00 CST) along with a more developed and well-mixed PBL.

HSRL-2 PBL heights retrieved at 12:00 and 15:00 CST include large areas over water, and lower r^2 values are seen at these times (Table 5 and Figure 8 for location reference), again highlighting the different correlations between land and water surfaces and corresponding PBL heights. Another source for bias between land and water surface simulated and observed PBL heights can be due to model land mask and land cover classifications. The model simulations will assign a water/land mask identity to each grid cell and a respective land cover classification (e.g., urban land, grassland, water body, and mixed forest). Land areas near bodies of water are typically impacted by this classification as a coastal grid cell, which contains both land and water surfaces, would be allocated to the water body classification and thus can be assigned too far offshore. The incorrect classification of land surfaces can cause simulations to underpredict surface fluxes and therefore PBL heights, for example, in Figures 8g and 8h near the Gulf of Mexico coast where lower PBL heights are simulated farther inland from shores compared to HSRL-2 observations. These nearshore regions show in large deviations (RMSE and MAE) for PBL heights calculated at 13:00, 14:00, and 15:00 CST in Table 5. In addition, in situ PBL observations show a more abrupt transition in coastal areas yet model simulations extend the transition areas over a larger onshore distance.

Comparisons between observed and modeled chemical concentrations are listed in Table 6. Figure 7 displays observed TCEQ CAMS hourly ozone values (circular markers) and hourly WRF-Chem outputs with background shading. Differences in ozone mixing ratios between the simulation and observations show a strong daytime/nighttime trend. While ozone is largely overpredicted during nighttime, it is significantly less so

Table 5
Correlation Coefficient (r^2), Root-Mean-Square Error (RMSE), Mean Absolute Error (MAE), Mean Bias, and Number of Comparisons (No.) for Hourly Simulated Versus Observed PBL Heights and for Hourly Simulated Versus Near-Surface Temperatures for 36 Ground Stations

Hour (CST)	PBL (m AGL)					Temperature (°C)			
	r^2	RMSE	MAE	Mean bias	No.	r^2	RMSE	MAE	Mean bias
7	0.35	79.2	70.3	56.4	27	0.1	1.6	1.1	−0.5
8	0.01	207.8	187.2	−185	222	0.1	2.1	1.7	−1.5
9	0.03	145.2	121.1	−80.6	289	0.0	1.7	1.3	−1.2
10	0.28	124.4	107.4	23.1	277	0.0	1.4	0.9	−0.7
12	0.08	82.6	60	52.7	40	0.5	1.0	0.7	−0.4
13	0.7	711.3	608.9	−584.1	175	0.6	1.0	0.7	−0.5
14	0.63	739	631	−618	262	0.5	1.2	0.8	−0.5
15	0.38	959.1	645	−612.6	305	0.6	1.1	0.9	−0.4

Note. Only hours for which simultaneous HSRL-2 and temperature comparisons could be calculated are shown.

Table 6
Comparisons Between Hourly Observed and Simulated O_3, NO_2, and NO Mixing Ratios (ppbv)

| Hour (CST)	O$_3$				NO$_2$				NO			
	r^2	Bias	MAE	RMSE	r^2	Bias	MAE	RMSE	r^2	Bias	MAE	RSME
7	0.28	19.60	19.90	21.41	0.79	−1.57	5.14	6.82	0.38	−41.90	41.90	64.17
8	0.27	11.17	12.20	14.71	0.50	−3.64	7.47	9.71	0.11	−9.49	11.11	19.74
9	0.18	4.25	11.12	13.72	0.41	−2.80	7.55	10.50	0.09	−1.37	6.83	12.18
10	0.05	3.58	9.62	12.98	0.36	−7.15	9.47	13.92	0.06	−0.51	2.75	4.43
11	0.00	1.41	10.61	14.06	0.22	−5.21	7.40	10.96	0.00	0.17	1.23	1.90
12	0.00	1.32	14.28	20.90	0.17	−1.84	4.14	5.76	0.03	0.25	0.91	1.13
13	0.40	3.11	11.79	16.59	0.05	−1.78	3.83	4.84	0.02	−0.00	0.64	0.89
14	0.42	4.87	10.13	13.55	0.06	−0.90	2.84	3.79	0.01	0.15	0.39	0.56
15	0.44	6.03	9.87	12.10	0.08	−1.35	2.85	3.97	0.00	−0.05	0.45	0.77

Note. Correlation coefficient (r^2), mean bias (Bias), mean average error (MAE), and root-mean-square error (RSME) displayed for each chemical species.

during daytime. During nighttime and early morning hours (0:00–07:00 CST) ozone values do not reach the observed low concentrations and also result in an overall overestimation of ozone further decreasing correlations (bias from 30.4 to 19.6 ppbv; Supporting Information). This is likely due to poor nighttime representation in some parameters of air quality models such as underestimation of dry deposition that can lead to an overestimation of nighttime ground level O_3 (Chen et al., 2008; Cuchiara et al., 2014; Lin & McElroy, 2010; Mao et al., 2006). During daytime, low correlations between observations and simulated ozone are seen, yet mean biases remain low indicating that poor correlations are more likely due to the simulation of ozone production rates and less likely due to the spatial distribution of ozone (see Supporting Information). As ozone values begin to increase later in the day (13:00–15:00 CST), correlation increases ($r^2 \approx 0.4$) with the Houston area experiencing widespread high ozone concentrations (Figures 7g–7i). Yet, the modeled concentrations for the western Galveston Bay sites (Figure 7) do not reach hourly mixing ratios as high as those observed (for example, La Porte in Figures 3h and 3l). See Supporting Information for further precursor discussion.

As HSRL-2 observations show the aerosol distribution over the Galveston Bay, we use the WRF-Chem simulation to explore the atmospheric dynamics in that area, which may impact pollutant distribution and concentrations. Figure 9 displays a vertical cross section (blue line in Figure 1) with simulated ozone concentrations and a two-dimensional wind field to show flows over the Galveston Bay along the same trajectory as that taken by the HSRL. Figures 9a–9d at 07:00–10:00 CST show an area of high ozone, likely the remains of the nighttime residual layer above the growing convective mixing layer. The ozone simulations and the observations from the TOPAZ lidar (Figure 10) agree quite well in the early morning hours, both in terms of magnitude and vertical extent. The modeled ozone mixing ratios reach about 67 ppbv between ~500 and 1,660 m AGL, while TOPAZ observed mixing ratios of ≈66 ppbv between ~500 and 2,000 m AGL (note the height limitation of 2,000 m). At 12:00 CST Figure 9f shows decreasing wind speeds and increasing ozone values near the surface likely due to daytime photochemical ozone formation coinciding with pollutant accumulation during calm winds (i.e., stagnant conditions, indicative of the convergence of the bay breeze and the synoptic flow). In contrast, observations at the La Porte site show this calm wind period at about 10:00 CST (Figure 3j), approximately 2 hr before the WRF-Chem simulation. Following this period, Figures 9g, 9h, and 9i (13:00, 14:00, and 15:00 CST) indicate continued recirculation of flows with an easterly bay breeze at low altitudes and a westerly return flow aloft with boundary between these flows consistently reaching lower altitudes. In addition to horizontal advection and ozone production rates, any potential downward mixing of RL remains, the additional buildup of pollutants during the stagnation period, and mixing between recirculation flows can contribute to the high surface ozone measurements to values as high as seen in the observations.

Figure 9j at 16:00 CST shows a similar polluted layer than that of HSRL-2 observations in Figure 5a measured at ~14:00 CST extending offshore over the Galveston Bay. Figure 9k at 17:00 CST indicated enhanced vertical suppression of the boundary between flows, which likely explains the next HSRL-2 transect in Figure 5b at ~15:00 CST where pollutants are observed farther down to lower altitudes. Figures 9i–9k indicate high ozone concentrations increasingly reaching lower altitudes over the Galveston Bay supporting the
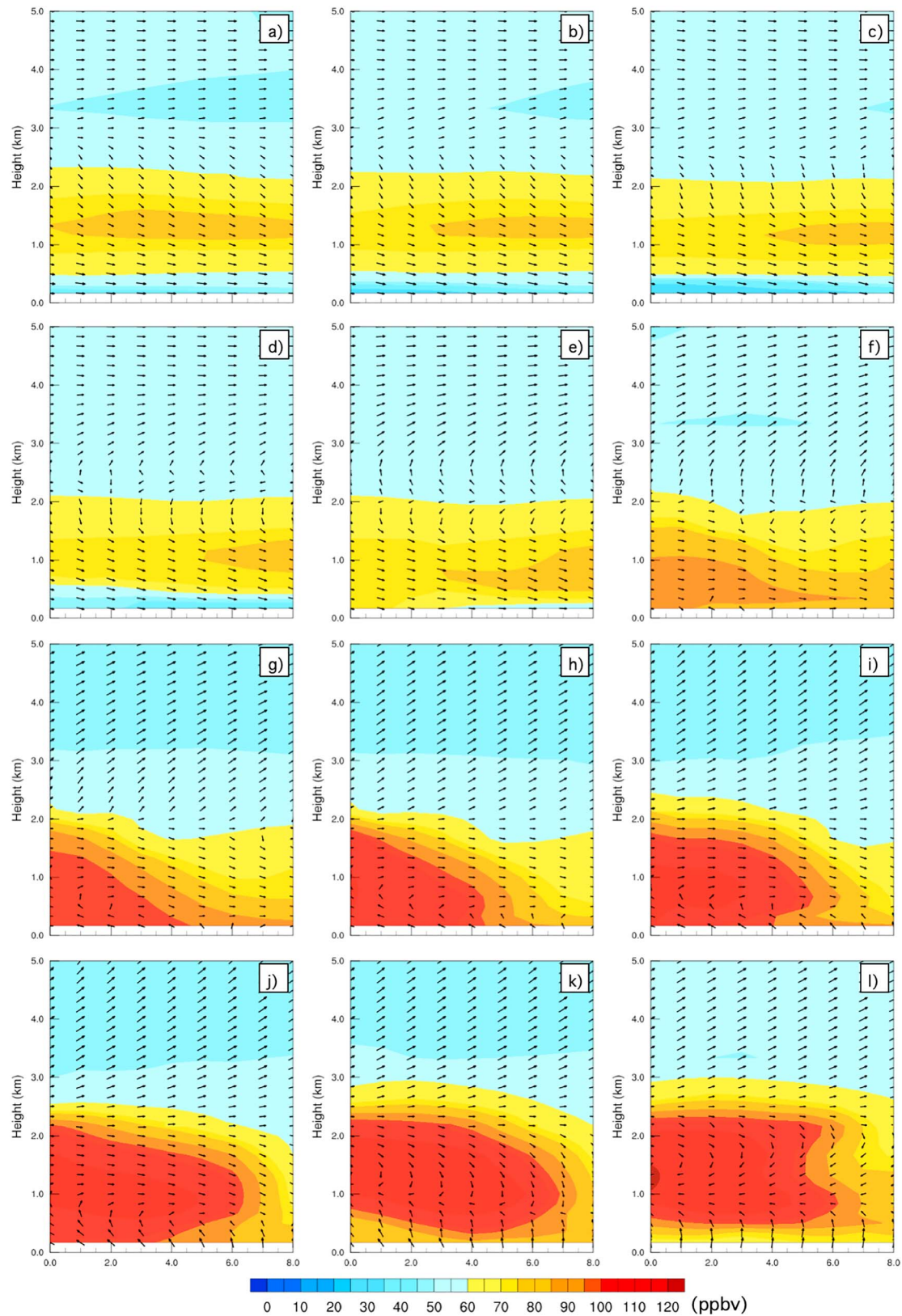
Figure 9. WRF-Chem O$_3$ mixing ratios and two-dimensional wind fields along the cross section over the Galveston Bay from the La Porte to Smith Point sites for 07:00 (a), 08:00 (b), 09:00 (c), 10:00 (d), 11:00 (e), 12:00 (f), 13:00 (g), 14:00 (h), 15:00 CST (i), 16:00 CST (j), 17:00 CST (k), and 18:00 CST (l) on 25 September 2013. *X* axis denotes model grid cells along cross section.
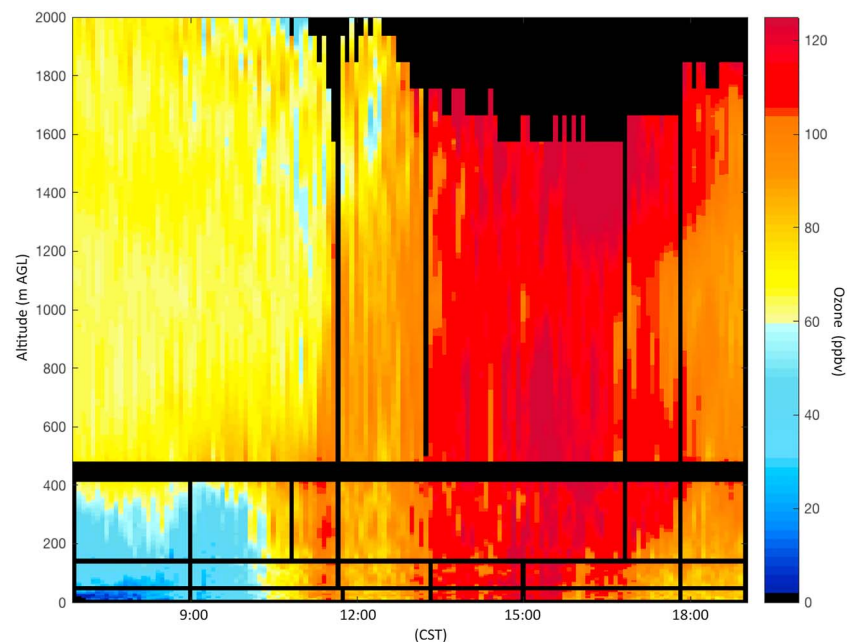
Figure 10. Ozone time-height cross section as obtained from the TOPAZ ozone lidar on 25 September 2013.

HSRL-2 observations. Contrarily to Figure 5b, however, near-water surface areas do not display an area of cleaner air; instead, ozone concentrations remain at ~80 ppbv and higher. Figure 9l displays the arrival of the simulated gulf breeze to the Galveston Bay area at 18:00 CST approximately 2 hr after observations.

Overall, the meteorological simulation setup for this case study is able to portray typical conditions conductive to high ozone events with the largest bias due to known simulation errors of overpredicted nighttime wind speeds over ocean surfaces and overpredicted nighttime ozone. As the model follows the observations closely (although with a slight sea/bay breeze delay), we can infer that the localized observed high ozone concentrations can be significantly driven by the local thermodynamically induced atmospheric circulation. In line with observations, model simulations show consistent downward motion of lofted flows over the bay and could hint at additional ozone enhancement from vertical downmixing of ozone remnants of both the nighttime residual layer during morning hours (7:00–10:00 CST; Figures 9a–9d) and from offshore return flow after the onset of the bay breeze (13:00–17:00 CST; Figures 9g–9k).

4. Summary and Conclusions

A case study for a high ozone event during land and sea/bay breeze circulations using a combination of in situ sampling, ground-based remote sensing, airborne measurements, and numerical model simulation (WRF-Chem) is presented. TCEQ air quality monitoring network stations, airborne lidar data from the NASA DISCOVER-AQ Texas 2013 campaign, and additional ground-based lidar instrumentation deployed during the campaign allowed for a spatial and temporal study of the progression of both meteorological and air quality conditions in the Houston-Galveston regions on 25 September 2013. The unique combination of observations and model simulations elucidated the complex interactions between circulation regimes and their impact on air quality in a coastal region.

Observations revealed localized high ozone mixing ratios reaching 151-ppbv near-western-Galveston Bay shores. These locations experienced a recirculation of air masses through the onset of the bay breeze (~11:00 CST) and lofted offshore return flows. Airborne nadir measurements of aerosol backscatter indicate a sequence in both time and space of continuous horizontal and vertical advection of an offshore return flow above the bay breeze extending over the Galveston Bay. This return flow is then progressively seen to reach lower altitudes pointing toward potential vertical downmixing observed between ~13:00 and 15:00 CST.

In addition, the horizontal and vertical advection of the lofted return flow revealed a limitation to aerosol backscatter retrieval of the PBL height in a marine environment with low aerosol loading. In this

environment retrieval algorithms are unable to properly detect the marine PBL and instead identify the top of the offshore return flow with higher aerosol content as the PBL height. As all retrieval methods search for a negative gradient in aerosol backscatter, the positive gradient above the clean marine layer would not be identified by any currently available algorithm. Furthermore, this highlights the differences between a thermodynamically identified PBL height and those retrieved from aerosol backscatter negative gradients. Assumptions of lidar retrievals must be reevaluated in similar cases, when a positive gradient is created by the development of the land/sea circulations but could be potentially important in other complex environment such as mountainous regions.

Model simulations using WRF-Chem showed overall reasonable agreement to observations in simulated PBL heights, near-surface temperatures, and surface ozone mixing ratios (Table 3). However, the onset of the sea/bay breeze was simulated 2 hr behind observations. These delays are critical and could indicate an area of inadequate simulation of land/sea recirculation that could impact the accuracy of air quality forecasts. Coastal regions where land/sea circulations play an important role in air quality must consider the implications of these delays for the air quality forecasting. Although overall correlations for the case study found reasonable agreement between model and observations, hourly comparisons revealed low correlations yet relatively low bias for comparison of PBL heights, near-surface temperatures, and air quality parameters (Tables 5 and 6). This suggests that spatial distribution is most likely the reason for low correlations. This was confirmed by dividing comparisons over land, the Gulf of Mexico and Galveston Bay (Table 4). PBL heights agreed well with observations over the Gulf of Mexico, underestimated over land surfaces, and underestimated over the Galveston Bay due to the identification of the return flow by the HSRL-2 retrievals. Although a high ozone event was simulated by WRF-Chem, the localized high ozone seen in surface measurements along the western shore of Galveston Bay was not simulated to the level of observations. This is likely due to the simulated delays in onset of bay breeze after peak ozone production hours. Model-simulated residual layer ozone concentrations agreed quite well with the TOPAZ ozone lidar observations; however, there were some differences in the vertical distribution of the residual layer ozone. Air quality resolutions using higher vertical and horizontal resolutions may be required for a better representation of the residual layer in order to successfully account of any residual layer contributions.

Observations revealed vertical downmixing from (1) the remnants of the nighttime residual layer during morning hours into the convective boundary layer and (2) from the lofted offshore return flow into the subjacent bay breeze flow. This was supported by the fairly homogeneous vertical structure of aerosols and ozone during the day. The magnitudes of these contributions, however, still need to be further evaluated and could be an important influence on surface pollutant concentrations in coastal environments as these regions tend to contain significant amount of pollutants.

References

Alvarez, R. J., Senff, C. J., Langford, A. O., Weickmann, A. M., Law, D. C., Machol, J. L., et al. (2011). Development and application of a compact, tunable, solid-state airborne ozone lidar system for boundary layer profiling. *Journal of Atmospheric and Oceanic Technology*, *28*(10), 1258–1272. https://doi.org/10.1175/JTECH-D-10-05044.1

Alvarez, R. J., Senff, C. J., Weickmann, A. M., Sandberg, S. P., Langford, A. O., Marchbanks, R. D., et al. (2012). Reconfiguration of the NOAA TOPAZ lidar for ground-based measurement of ozone and aerosol backscatter, Proceedings of the 26th International Laser Radar Conference, Porto Heli, Greece.

Angevine, W. M., Tjernström, M., & Žagar, M. (2006). Modeling of the coastal boundary layer and pollutant transport in New England. *Journal of Applied Meteorology and Climatology*, *45*(1), 137–154. https://doi.org/10.1175/JAM2333.1

Baars, H., Ansmann, A., Engelmann, R., & Althausen, D. (2008). Continuous monitoring of the boundary-layer top with lidar. *Atmospheric Chemistry and Physics*, *8*(23), 7281–7296. https://doi.org/10.5194/acp-8-7281-2008

Baker, K. R., Misenis, C., Obland, M. D., Ferrare, R. A., Scarino, A. J., & Kelly, J. T. (2013). Evaluation of surface and upper air fine scale WRF meteorological modeling of the May and June 2010 CalNex period in California. *Atmospheric Environment*, *80*, 299–309. https://doi.org/10.1016/j.atmosenv.2013.08.006

Banta, R. M., Senff, C. J., Nielsen-Gammon, J., Darby, L. S., Ryerson, T. B., Alvarez, R. J., et al. (2005). A bad air day in Houston. *Bulletin of the American Meteorological Society*, *86*(5), 657–670. https://doi.org/10.1175/BAMS-86-5-657

Bao, J. W., Michelson, S. A., McKeen, S. A., & Grell, G. A. (2005). Meteorological evaluation of a weather-chemistry forecasting model using observations from the TEXAS-AQS 2000 field experiment. *Journal of Geophysical Research*, *110*, D21105. https://doi.org/10.1029/2004JD005024

Brooks, I. M. (2003). Finding boundary layer top: Application of a wavelet covariance transform to lidar backscatter profiles. *Journal of Atmospheric and Oceanic Technology*, *20*(8), 1092–1105. https://doi.org/10.1175/1520-0426(2003)020<1092:FBLTAO>2.0.CO;2

Caicedo, V., Rappenglueck, B., Lefer, B., Morris, G., Toledo, D., & Delgado, R. (2017). Comparison of aerosol LIDAR retrieval methods for boundary layer height detection using ceilometer backscatter data. *Atmospheric Measurement Techniques*, *10*(4), 1609–1622. https://doi.org/10.5194/amt-10-1609-2017

Campbell, J. R., Hlavka, D. L., Welton, E. J., Flynn, C. J., Turner, D. D., Spinhirne, J. D., et al. (2002). Full-time, eye-safe cloud and aerosol lidar observation at atmospheric radiation measurement program sites: Instruments and data processing. *Journal of Atmospheric and Oceanic Technology*, *19*(4), 431–442. https://doi.org/10.1175/1520-0426(2002)019<0431:FTESCA>2.0.CO;2

Chen, F., Miao, S., Tewari, M., Bao, J.-W., & Kusaka, H. (2011). A numerical study of interactions between surface forcing and sea-breeze circulations and their effects on stagnation in the greater Houston area. *Journal of Geophysical Research*, *116*, D12105. https://doi.org/10.1029/2010JD015533

Chen, J., Vaughan, J., Avise, J., O'Neill, S., & Lamb, B. (2008). Enhancement and evaluation of the AIRPACT ozone and PM2.5 forecast system for the Pacific Northwest. *Journal of Geophysical Research*, *113*, D14305. https://doi.org/10.1029/2007JD009554

Cheng, Y., & Steenburgh, J. (2005). Evaluation of surface sensible weather forecasts by the WRF and the eta models over the Western United States. *Weather Forecast*, *20*(5), 812–821. https://doi.org/10.1175/WAF885.1

Cohn, S., & Angevine, W. (2000). Boundary layer height and entrainment zone thickness measured by lidars and wind-profiling radars. *Journal of Applied Meteorology*, *39*(8), 1233–1247. https://doi.org/10.1175/1520-0450(2000)039<1233:BLHAEZ>2.0.CO;2

Compton, J. C., Delgado, R., Berkoff, T. A., & Hoff, R. M. (2013). Determination of planetary boundary layer height on short spatial and temporal scales: A demonstration of the covariance wavelet transform in ground-based wind profiler and lidar measurements. *Journal of Atmospheric and Oceanic Technology*, *30*(7), 1566–1575. https://doi.org/10.1175/JTECH-D-12-00116.1

Cuchiara, G. C., Li, X., Carvalho, J., & Rappenglück, B. (2014). Intercomparison of planetary boundary layer parameterization and its impacts on surface ozone concentration in the WRF/Chem model for a case study in Houston/Texas. *Atmospheric Environment*, *96*, 175–185. https://doi.org/10.1016/j.atmosenv.2014.07.013

Czader, B. H., Li, X., & Rappenglück, B. (2013). CMAQ modeling and analysis of radicals, radical precursors, and chemical transformations. *Journal of Geophysical Research: Atmospheres*, *118*, 11,376–11,387. https://doi.org/10.1002/jgrd.50807

Darby, L. S. (2005). Cluster analysis of surface winds in Houston, Texas, and the impact of wind patterns on ozone. *Journal of Applied Meteorology and Climatology*, *44*(12), 1788–1806. https://doi.org/10.1175/JAM2320.1

Darby, L. S., McKeen, S. A., Senff, C. J., White, A. B., Banta, R. M., Post, M. J., et al. (2007). Ozone differences between near-coastal and offshore sites in New England: Role of meteorology. *Journal of Geophysical Research*, *112*, D16S91. https://doi.org/10.1029/2007JD008446

Davis, K. J., Gamage, N., Hagelberg, C. R., Kiemle, C., Lenschow, D. H., & Sullivan, P. P. (2000). An objective method for deriving atmospheric structure from airborne lidar observations. *Journal of Atmospheric and Oceanic Technology*, *17*(11), 1455–1468. https://doi.org/10.1175/1520-0426(2000)017<1455:AOMFDA>2.0.CO;2

Day, B. M., Rappenglück, B., Clements, C. B., Tucker, S. C., & Brewer, W. A. (2010). Nocturnal boundary layer characteristics and land breeze development in Houston, Texas, during TexAQS-II. *Atmospheric Environment*, *44*(33), 4014–4023. https://doi.org/10.1016/j.atmosenv.2009.01.031.

DISCOVER-AQ Science Team (2014). DISCOVER-AQ P-3B [Data set]. NASA Langley Atmospheric Science Data Center DAAC. https://doi.org/10.5067/aircraft/discover-aq/aerosol-tracegas

Emmons, L. K., Walters, S., Hess, P. G., Lamarque, J. F., Pfister, G. G., Fillmore, D., et al. (2010). Description and evaluation of the Model for Ozone and Related chemical Tracers, version 4 (MOZART-4). *Geoscientific Model Development*, *3*(1), 43–67. https://doi.org/10.5194/gmd-3-43-2010

Fast, J. D., Gustafson, W. I., Easter, R. C., Zaveri, R. A., Barnard, J. C., Chapman, E. G., et al. (2006). Evolution of ozone, particulates, and aerosol direct radiative forcing in the vicinity of Houston using a fully coupled meteorology-chemistry-aerosol model. *Journal of Geophysical Research*, *111*, D21305. https://doi.org/10.1029/2005JD006721

Gangoiti, G., Alonso, L., Navazo, M., Albizuri, A., Perez-Landa, G., Matabuena, M., et al. (2002). Regional transport of pollutants over the Bay of Biscay: Analysis of an ozone episode under a blocking anticyclone in west-central Europe. *Atmospheric Environment*, *36*(8), 1349–1361. https://doi.org/10.1016/S1352-2310(01)00536-2

Hegarty, J. D., Lewis, J., McGrath-Spangler, E. L., Henderson, J., Scarino, A. J., DeCola, P., et al. (2018). Analysis of the planetary boundary layer height during DISCOVER-AQ Baltimore–Washington, D.C., with lidar and high-resolution WRF modeling. *Journal of Applied Meteorology and Climatology*, *57*(11), 2679–2696. https://doi.org/10.1175/JAMC-D-18-0014.1

Hong, S.-Y., Noh, Y., & Dudhia, J. (2006). A new vertical diffusion package with an explicit treatment of entrainment processes. *Monthly Weather Review*, *134*(9), 2318–2341. https://doi.org/10.1175/MWR3199.1

Hu, X.-M., Nielsen-Gammon, J. W., & Zhang, F. (2010). Evaluation of three planetary boundary layer schemes in the WRF model. *Journal of Applied Meteorology and Climatology*, *49*(9), 1831–1844. https://doi.org/10.1175/2010JAMC2432.1

Lin, J.-T., & McElroy, M. (2010). Impacts of boundary layer mixing on pollutant vertical profiles in the lower troposphere: Implications to satellite remote sensing. *Atmospheric Environment*, *44*(14), 1726–1739. https://doi.org/10.1016/j.atmosenv.2010.02.009

Loughner, C. P., Tzortziou, M., Follette-Cook, M., Pickering, K. E., Goldberg, D., Satam, C., et al. (2014). Impact of bay-breeze circulations on surface air quality and boundary layer export. *Journal of Applied Meteorology and Climatology*, *53*(7), 1697–1713. https://doi.org/10.1175/JAMC-D-13-0323.1

Mao, Q., Gautney, L. L., Cook, T. M., Jacobs, M. E., Smith, S. N., & Kelsoe, J. J. (2006). Numerical experiments on MM5-CMAQ sensitivity to various PBL schemes. *Atmospheric Environment*, *40*, e3092–e3110.

Martins, D. K., Stauffer, R., Thompson, A. M., Pippin, M., & Knepp, T. (2012). Surface ozone at a coastal suburban site in 2009 and 2010: Relationships to chemical and meteorological processes. *Journal of Geophysical Research*, *117*, D05306. https://doi.org/10.1029/2011JD016828

McElroy, J. L., & Smith, T. B. (1991). Lidar descriptions of mixing-layer thickness characteristics in a complex terrain/coastal environment. *Journal of Applied Meteorology and Climatology*, *30*(5), 585–597. https://doi.org/10.1175/1520-0450(1991)030<0585:LDOMLT>2.0.CO;2

Misenis, C., Hu, X., Krishnan, S., Zhang, Y., Fast, J. D (2006). Sensitivity of WRF/CHEM predictions to meteorological schemes. In: 86th Annual AMS Conference and the 14th Joint Conference on the Applications of Air Pollution Meteorology with the A&WMA, Atlanta/GA, USA.

Münkel, C., Eresmaa, N., Räsänen, J., & Karppinen, A. (2007). Retrieval of mixing height and dust concentration with lidar ceilometer. *Bound.-Lay. Meteorology*, *124*(1), 117–128. https://doi.org/10.1007/s10546-0069103-3

Ngan, F., Byun, D., Kim, H., Lee, D., Rappenglück, B., & Pour-Biazar, A. (2012). Performance assessment of retrospective meteorological inputs for use in air quality modeling during TexAQS 2006. *Atmospheric Environment*, *54*, 86–96. https://doi.org/10.1017/j.atmosenv.2012.01.035

Pendergrass, W. R., Myles, L., Vogel, C. A., Anjaneyulu, Y., Dodla, V. B. R., Dasari, H. P., et al. (2010). Observation, analysis, and modeling of the sea-breeze circulation during the NOAA/ARL-JSU meteorological field experiment summer 2009. Proc. 90th Annual Meeting of the American Met. Society Conf. Atlanta, GA, USA.

Rappenglück, B., Perna, R., Zhong, S., & Morris, G. A. (2008). An analysis of the vertical structure of the atmosphere and the upper-level meteorology and their impact on surface ozone levels in Houston, Texas. *Journal of Geophysical Research*, *113*, D17315. https://doi.org/10.1029/2007JD009745

Roux, G., Liu, Y., Monache, L. D., Sheu, R. Y., Warner, T. T. (June 2009). Verification of high resolution WRF-RTFDDA surface forecasts over mountains and plains. In: 10th WRF Users' Workshop, Boulder, Colorado, USA

Scarino, A. J., Obland, M. D., Fast, J. D., Burton, S. P., Ferrare, R. A., Hostetler, C. A., et al. (2014). Comparison of mixed layer heights from airborne High Spectral Resolution Lidar, ground-based measurements, and the WRF-Chem model during CalNex and CARES. *Atmospheric Chemistry and Physics*, *14*(11), 5547–5560. https://doi.org/10.5194/acp-14-5547-2014

Seibert, P., Beyrich, F., Gryning, S. E., Joffre, S., Rasmussen, A., & Tercier, P. (2000). Review and intercomparison of operational methods for the determination of the mixing height. *Atmospheric Environment*, *34*(7), 1001–1027. https://doi.org/10.1016/S1352-2310(99)00349-0

Stauffer, R. M., & Thompson, A. M. (2015). Bay-breeze climatology at two sites along the Chesapeake Bay from1986-2010: Implications for surface ozone. *Journal of Atmospheric Chemistry*, *72*(3-4), 355–372. https://doi.org/10.1007/s10874-013-9260-y

Stauffer, R. M., Thompson, A. M., Martins, D. K., Clark, R. D., Goldberg, D. L., Loughner, C. P., et al. (2013). Bay-breeze influence on surface ozone at Edgewood, MD during July 2011. *Journal of Atmospheric Chemistry*, *72*(3-4), 355–372. https://doi.org/10.1007/s10874-013-9260-y

Steele, C. J., Dorling, S. R., von Glasow, R., & Bacon, J. (2013). Idealized WRF model sensitivity simulations of sea-breeze types and their effects on offshore wind fields. *Atmospheric Chemistry and Physics*, *13*(1), 443–461. https://doi.org/10.5194/acp-13-443-2013

Steyn, D. G., Baldi, M., & Hoff, R. M. (1999). The detection of mixed layer depth and entrainment zone thickness from lidar backscatter profiles. *Journal of Atmospheric and Oceanic Technology*, *16*(7), 953–959. https://doi.org/10.1175/1520-0426(1999)016<0953:TDOMLD>2.0.CO;2

Strawbridge, K. B., & Snyder, B. J. (2004). Planetary boundary layer height determination during Pacific 2001 using the advantage of a scanning lidar instrument. *Atmospheric Environment*, *38*(34), 5861–5871. https://doi.org/10.1016/j.atmosenv.2003.10.065

Tijm, A. B. C., Holtslag, A. A. M., & van Delden, A. J. (1999). Observations and modeling of the sea-breeze with the return current. *Monthly Weather Review*, *127*(5), 625–640. https://doi.org/10.1175/1520-0493(1999)127<0625:OAMOTS>2.0.CO;2

Uzan, L., Egert, S., & Alpert, P. (2016). Ceilometer evaluation of the eastern Mediterranean summer boundary layer height—First study of two Israeli sites. *Atmospheric Measurement Techniques*, *9*(9), 4387–4398. https://doi.org/10.5194/amt-9-4387-2016

Wilmot, C.-S. M., Rappenglück, B., Li, X., & Cuchiara, G. (2014). MM5 v3.6.1 and WRF v3.5.1 model comparison of standard and surface energy variables in the development of the planetary boundary layer. *Geoscientific Model Development*, *7*(6), 2693–2707. https://doi.org/10.5194/gmd-7-2693-2014

Wu, Y.-L., Lin, C.-H., Lai, C.-H., Lai, H.-C., & Young, C.-Y. (2010). Effects of local circulations, turbulent internal boundary layers, and elevated industrial plumes on coastal ozone pollution in the downwind Kaohsiung urban-industrial complex. *Terrestrial, Atmospheric and Oceanic Sciences*, *21*(2), 343–357. https://doi.org/10.3319/TAO.2009.04.14.01(A)

Yerramilli, A., Challa, V., Dodla, V., Dasari, H., Young, J., Patrick, C., et al. (2010). Simulation of surface ozone pollution in the central Gulf Coast region using WRF/Chem model: Sensitivity to PBL and land surface physics. *Advances in Meteorology*, *2010*, 1e24. https://doi.org/10.115/2010/319138

Zhang, F., Bei, N., Nielsen-Gammon, J. W., Li, G., Zhang, R., Stuart, A., & Aksoy, A. (2007). Impacts of meteorological uncertainties on ozone pollution predictability estimated through meteorological and photochemical ensemble forecasts. *Journal of Geophysical Research*, *112*, D04304. https://doi.org/10.1029/2006JD007429

References From the Supporting Information

Berkoff, T. A., Welton, E. J., Campbell, J. R., Scott, V. S., & Spinhirne, J. D. (2003). Investigation of overlap correction techniques for the Micro-Pulse Lidar NETwork (MPLNET). Proc. Geoscience and Remote Sensing Symp. 2003, IGARSS'03, Toulouse, France, IEEE International, Vol. 7, 4395–4397, https://doi.org/10.1109/IGARSS.2003.1295527

Hair, J. W., Hostetler, C. A., Cook, A. L., Harper, D. B., Ferrare, R. A., Mack, T. L., et al. (2008). Airborne High Spectral Resolution Lidar for profiling aerosol optical properties. *Applied Optics*, *47*(36), 6734–6752. https://doi.org/10.1364/AO.47.006734

Kotthaus, S., O'Connor, E., Münkel, C., Charlton-Perez, C., Haeffelin, M., Gabey, A. M., & Grimmond, C. S. B. (2016). Recommendations for processing atmospheric attenuated backscatter profiles from Vaisala CL31 ceilometers. *Atmospheric Measurement Techniques*, *9*(8), 3769–3791. https://doi.org/10.5194/amt-9-3769-2016

Rogers, R. R., Hair, J. W., Hostetler, C. A., Ferrare, R. A., Obland, M. D., Cook, A. L., et al. (2009). NASA LaRC airborne High Spectral Resolution Lidar aerosol measurements during MILAGRO: Observations and validation. *Atmospheric Chemistry and Physics*, *9*(14), 4811–4826. https://doi.org/10.5194/acp-9-4811-2009

Sawamura, P., Moore, R. H., Burton, S. P., Chemyakin, E., Müller, D., Kolgotin, A., et al. (2017). HSRL-2 aerosol optical measurements and microphysical retrievals vs. airborne in situ measurements during DISCOVER-AQ 2013: An intercomparison study. *Atmospheric Chemistry and Physics*, *17*(11), 7229–7243. https://doi.org/10.5194/acp-17-7229-2017

Sokół, P., Stachlewska, I. S., Ungureanu, I., & Stefan, S. (2014). Evaluation of the boundary layer morning transition using the CL-31 ceilometer signals. *Acta Geophysica*, *62*(2), 367–380. https://doi.org/10.2478/s11600-013-0158-5